ADVANCED FUNCTIONAL MATERIALS
www.afm-journal.de

Climbing Plant-Inspired Micropatterned Devices for Reversible Attachment

Isabella Fiorello, Omar Tricinci, Giovanna Adele Naselli, Alessio Mondini, Carlo Filippeschi, Francesca Tramacere, Anand Kumar Mishra, and Barbara Mazzolai**

Climbing plants have evolved over millions of years and have adapted to unpredictable scenarios in unique ways. These crucial features make plants an outstanding biological model for scientists and engineers. Inspired by the ratchet-like attachment mechanism of the hook-climber *Galium aparine*, a novel micropatterned flexible mechanical interlocker is fabricated using a 3D direct laser lithography technique. The artificial hooks are designed based on a morphometric analysis of natural hooks. They are characterized in terms of pull-off and shear forces, both in an array and as individual hooks. The microprinted hooks array shows high values of pull-off forces (up to $F_{\perp} \approx 0.4$ N cm^{-2}) and shear forces (up to $F_{//} \approx 13.8$ N cm^{-2}) on several rough surfaces (i.e., abrasive materials, fabrics, and artificial skin tissues). The contact separation forces of individual artificial hooks are estimated when loads with different orientations are applied (up to $F \approx 0.26$ N). In addition, a patterned tape with directional microhooks is integrated into a mobile platform to demonstrate its climbing ability on inclined surfaces of up to 45°. This research opens up new opportunities for prototyping the next generation of mechanical interlockers, particularly for soft- and microrobotics, the textile industry, and biomedical fields.

1. Introduction

One of the greatest challenges in robotics and engineering is to develop ingenious systems that can work in complex environments, managing unpredictable constraints.[1] Scientists have recently tried to solve such issues by developing solutions that are inspired by Nature.[2] Biologically inspired approaches are now being used to fabricate new smart solutions for gripping and anchoring. These solutions mimic the morphological features of the selected animals (e.g., the remora disc,[3] octopus sucker,[4] gecko foot,[5] insect pads),[6] and plants (e.g., trichomes).[7,8] A growing interest concerns the use of bioinspired architectures to develop novel materials for reversible attachment and detachment on different rough surfaces, using different strategies, such as mechanical interlocking,[9–11] van der Waals forces,[12–14] or suction cups[15] (see Table S1, Supporting Information, for a brief overview of the bioinspired structures for rough surfaces).

One of the main reversible attachment strategies includes the use of hook-like microstructures for generating high pull-off and friction forces on rough surfaces.[16] To date, the most famous hook-based mechanical interlocker is Velcro, which was inspired by burdock seeds. In addition, other anchoring systems for mechanical interlocking have been developed and have shown great potential, including probabilistic and fabric fasteners,[6,16,17] dry adhesives,[7] medical patches for skin interlocking,[10] and microspines for climbing robots[18–20] or grippers.[21,22]

Climbing plants have evolved unique adaptation and attachment abilities, which have enabled them to colonize several habitats.[23,24] A wonderful, albeit insidious, example of natural selection is the herbaceous climber *Galium aparine* L., which can grow in different habitats (such as arable fields, hedgerows, forests, and wastelands)[25] by attaching itself to several rough objects. This parasitic plant exploits its leaves, which are covered with microscopic hooks, to mechanically interlock itself to the host (Figure S1 and Movie S1, Supporting Information).[26,27] Although its hooks are present on both leaf surfaces, hooks on the adaxial (upper side) and abaxial (lower side) differ significantly in terms of structural and mechanical properties.[26] The result of this difference is a parasitic ratchet-like climbing mechanism (**Figure 1**a–c), which allows *G. aparine* L. to climb onto the sunlit side and simultaneously orient itself advantageously for photosynthesis (by stealing light from the host plant).[26,27]

I. Fiorello, Dr. O. Tricinci, Dr. G. A. Naselli, Dr. A. Mondini, C. Filippeschi, Dr. F. Tramacere, Dr. B. Mazzolai
Istituto Italiano di Tecnologia
Center for Micro-BioRobotics
Viale Rinaldo Piaggio 34, Pontedera, Pisa 56025, Italy
E-mail: isabella.fiorello@iit.it; barbara.mazzolai@iit.it
I. Fiorello
The BioRobotics Institute
Scuola Superiore Sant'Anna
Viale Rinaldo Piaggio 34, Pontedera, Pisa 56025, Italy
Dr. A. K. Mishra
Cornell University
Department of Mechanical and Aerospace Engineering
Ithaca, NY 14850, USA
The ORCID identification number(s) for the author(s) of this article can be found under https://doi.org/10.1002/admt.202003380.

DOI: 10.1002/adfm.202003380

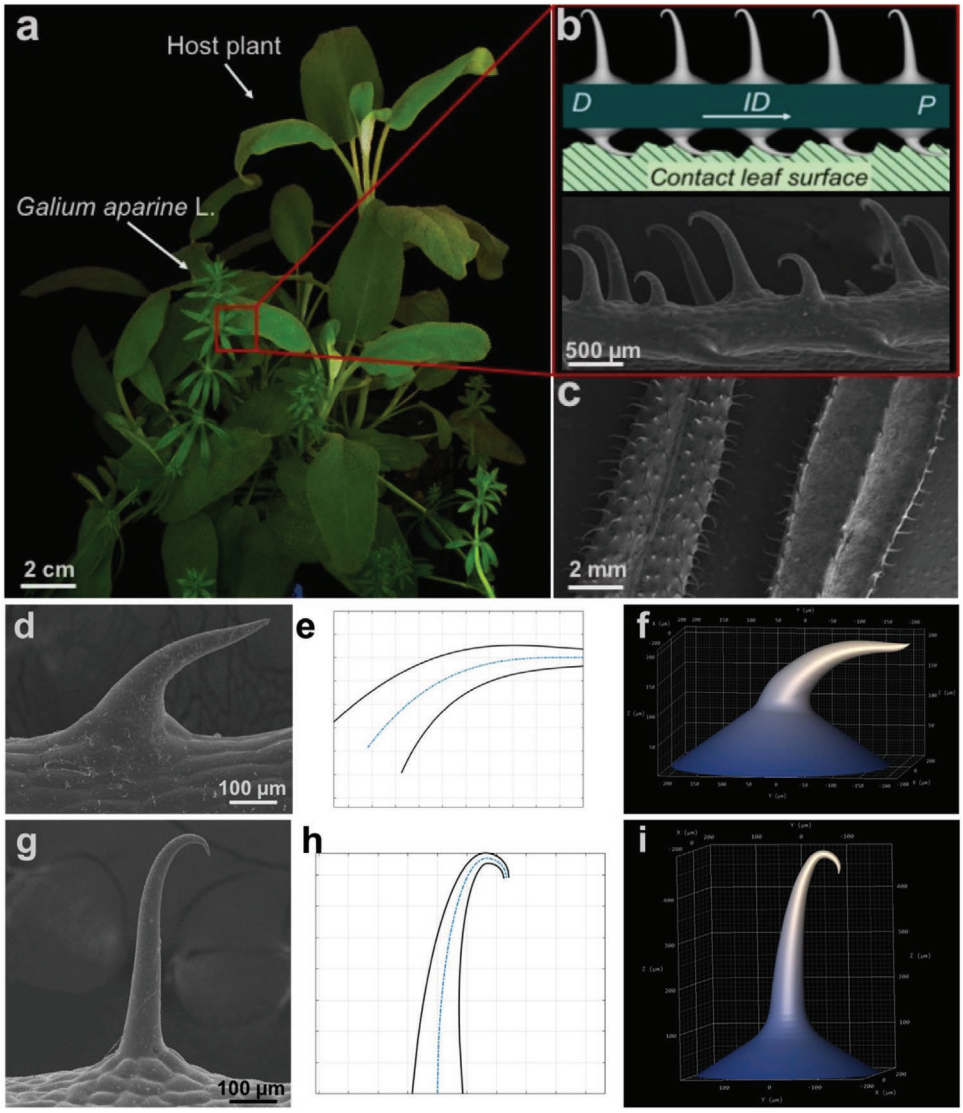

Figure 1. Bioinspired design and modeling of *G. aparine* leaf hooks. a) The cleaver *G. aparine* L. climbing up the host plant (*Salvia officinalis* L.). b) Details of the schematic (upper panel) and natural view (SEM images, lower panel) of the abaxial and adaxial sides of a *G. aparine* leaf. The arrow indicates the interlocking direction (ID) of the abaxial hooks over the contact leaf surface of the host plant. Distal (D) and proximal (P) parts of *G. aparine* leaf are reported. c) SEM pictures of the adaxial (left) and abaxial (right) side of natural leaves. d) Abaxial and g) adaxial hook (SEM images). Geometrical models for e) the abaxial and h) adaxial hooks. CAD models obtained in SolidWorks of f) the abaxial and i) adaxial hooks.

Inspired by the climbing mechanism of *G. aparine* L., we designed and developed a new type of flexible attachment device with 3D patterned hooks at the microscale. The geometry of the artificial hooks was obtained accounting for the characteristics of the natural hooks (e.g., shape and size) by exploiting a mathematical model based on curved beam theory[28] in order to guarantee structural integrity under assigned load conditions.

We fabricated the hooks using 3D direct laser lithography (DLL), which is based on multiphoton absorption.[29] DLL is a high-precision additive manufacturing technique for making 3D structures particularly for biomimetic materials, optics, micromechanics, and microrobotics.[30]

In this paper, we exploit the high reproducibility and scalability features of DLL in order to fabricate climbing plant-inspired patterned attachment devices at the microscale. The devices were tested, in terms of pull-off and shear forces, with various types of texture and roughness, including sandpaper, Velcro-loop fabric, polyester fabric, and artificial skin tissue. Pull-off experiments were also carried out to measure the contact separation force of an individual artificial hook with different load directions. Lastly, we demonstrated that a tape-like adhesive with direction-based abaxial microhooks can be integrated in a miniaturized mobile platform for climbing over inclined rough surfaces.

We believe that our climbing plant-inspired self-interlocking prototypes have great potential in several applications, such as micropatterned probabilistic fasteners for clothing, flexible dry adhesives for micro electro-mechanical systems, medical patches for skin interlocking, and climbing robots.

2. Results and Discussion

2.1. Design and Modeling of Bioinspired Leaf Hooks

We studied how *G. aparine* attaches its hooks onto a host plant (i.e., *Salvia officinalis* L.) by means of time-lapse observations (Movie S1, Supporting Information). *G. aparine* L. attaches itself onto the upper side of the host leaf surface (i.e., not underneath), using a self-tightening attachment mechanism (one surface ratcheting, the other surface slipping)[24,26] (Figure 1a,b). The adaxial leaf surfaces are completely covered with hooks, while on the abaxial side, the hooks are only in the center and at the edges (Figure 1c).[26] The morphology of abaxial and adaxial hooks differs both in shape and size[26] (Figure 1d,g, respectively).

We carried out a morphometric analysis of natural hooks via scanning electron microscope images, similarly to methods used in other studies on hooks, such as fruit burrs or prickles[31–33] (Figure S2 and Table S2, Supporting Information). Artificial hooks have already been designed to meet structural requirements by taking into account the geometrical parameters of natural hooks and selecting the most appropriate materials for microfabrication. Although Young's modulus (E) of *G. aparine* natural leaf hooks is not yet known, we selected the E range value of *G. aparine* fruit hooks ($E \approx 2.02$–23.20)[34] as a reference in order to identify the material for the fabrication of the artificial hooks, which is $E \approx 4.6$ GPa.

Figure 1e,h shows the profiles of the abaxial and adaxial hooks, respectively. For both, we used the beam theory to model the mechanical response of the hooks to an assigned load. For all the theoretical model details, see Equation (S1), Table S3, Figure S3, and Figure S4 in the Supporting Information. Based on the geometries obtained, we developed 3D solid models for the artificial abaxial and adaxial hooks (Figure 1f,i, respectively), which were used for the microfabrication.

2.2. Microfabrication of the Micropatterned Attachment Devices

We fabricated our microhooks using DLL in negative-tone photoresist (IP-S resin, a designed material for two-photon polymerization) on Mylar substrates (**Figure 2**a, see the Experimental Section for details). Mylar sheets were chosen above all because they are more flexible than traditional rigid substrates.[35] Artificial abaxial and adaxial hooks consist of a joint-like conical base and an upper hooked part which becomes thinner as it gets close to the apical part, mimicking the structure of the natural hooks. The upper part of the artificial abaxial hooks has a downward orientation, with a larger basal diameter (≈120 µm) than the adaxial hooks (≈95 µm) (Figure 2b–g). The arrays of artificial abaxial and adaxial hooks were arranged in a square of 6 by 6 structures, with a fixed center-to-center spacing of 800 µm. Overall, the DLL-made microstructures are characterized by high resolution and reproducibility, even at the tip (Figure 2b–g). In addition, the large contact area ensures that the structures are strongly attached onto the Mylar sheet, ($200 \cdot 200 \cdot \pi$ µm^2) and that laser speed and power are optimized (Movie S2, Supporting Information).

2.3. Pull-Off and Shear Properties of the Micropatterned Attachment Devices

Natural hooks attach well to a wide range of rough surfaces in nature[26,27,36] (e.g., Figure S1, Supporting Information). Similarly to the tiny hooks of burdock burrs, which inspired the conventional hook and loop Velcro mechanical interlocker,[11,37] the *G. aparine* abaxial and adaxial natural hooks can stick onto fabric textiles (Figure S5, Supporting Information).[26] However, unlike the hooked part of Velcro, our field and microscope observations show that *G. aparine* hooks can also anchor and penetrate inside rough skin tissue (Figure S5, Supporting Information). The performance of the hooks during interlocking strongly depends on three main factors: i) the size and shape of the hook, ii) the texture of the contact substrate, and iii) the preload applied.[6,26,31]

In the present work, we investigated the pull-off and shear attachment properties of the bioinspired artificial micropatterned prototypes on several surfaces with different degrees of roughness and/or textures (**Figure 3** and Figure S6, Table S4, and Movie S3, Supporting Information).

To the best of our knowledge, this is the first demonstration of the use of a climbing plant-like mechanical interlocker with normal and shear-induced attachments for a wide range of rough surfaces, ranging from fabrics to skin tissues.

2.3.1. Pull-Off Attachment Properties

Figure 4 reports the pull-off forces (Figure 3a, in caption I) of the abaxial and adaxial (Figure 4a,b, respectively) hook array by applying various preloads from 0.02 to 1 N on different rough substrates, including commercial textile fabrics with two different textures, i.e., 1) polyester fabric with "well-organized" woven fibers (Figure S6e, Supporting Information) and 2) Velcro-loop with "messy" looped fibers (Figure S6f, Supporting Information), and soft artificial skin tissues. As expected, the results showed that the attachment strength of both abaxial and adaxial hooks are influenced by the normal preload and by the type of substrate used for the tests (Figure 4a,b). The higher the preload (up to a maximum value of 1 N because higher preload significantly modifies the hooks morphology affecting, in turn, the attachment measurements), the greater the detachment forces, due to the higher number of hooks that interlock with the contact substrate. In contrast, the preload does not seem to affect the detachment strength of the hooks on looped fabric (Figure 4a,b).

Preload-dependent reversible mechanical interlocking, both in normal and shear directions, has also been reported in beetle-inspired wing-locking devices, where higher preloads induce a major overlapping of the high aspect ratio micro- and nanopillars amplified by attractive van der Waals force-mediated interlocking.[13]

In our study, the highest detachment strength of the abaxial hook array ranged from 0.15 ± 0.03 N cm^{-2} for artificial skin to 0.39 ± 0.14 N cm^{-2} for polyester fabrics (Figure 4a). On the other hand, the maximum detachment forces of the adaxial hook array ranged from 0.05 ± 0.01 N cm^{-2} for Velcro-loop fabrics to 0.24 ± 0.04 N cm^{-2} for polyester fabrics (Figure 4b).

The abaxial hooks showed higher detachment forces respect to the adaxial ones, resembling the natural counterpart. This

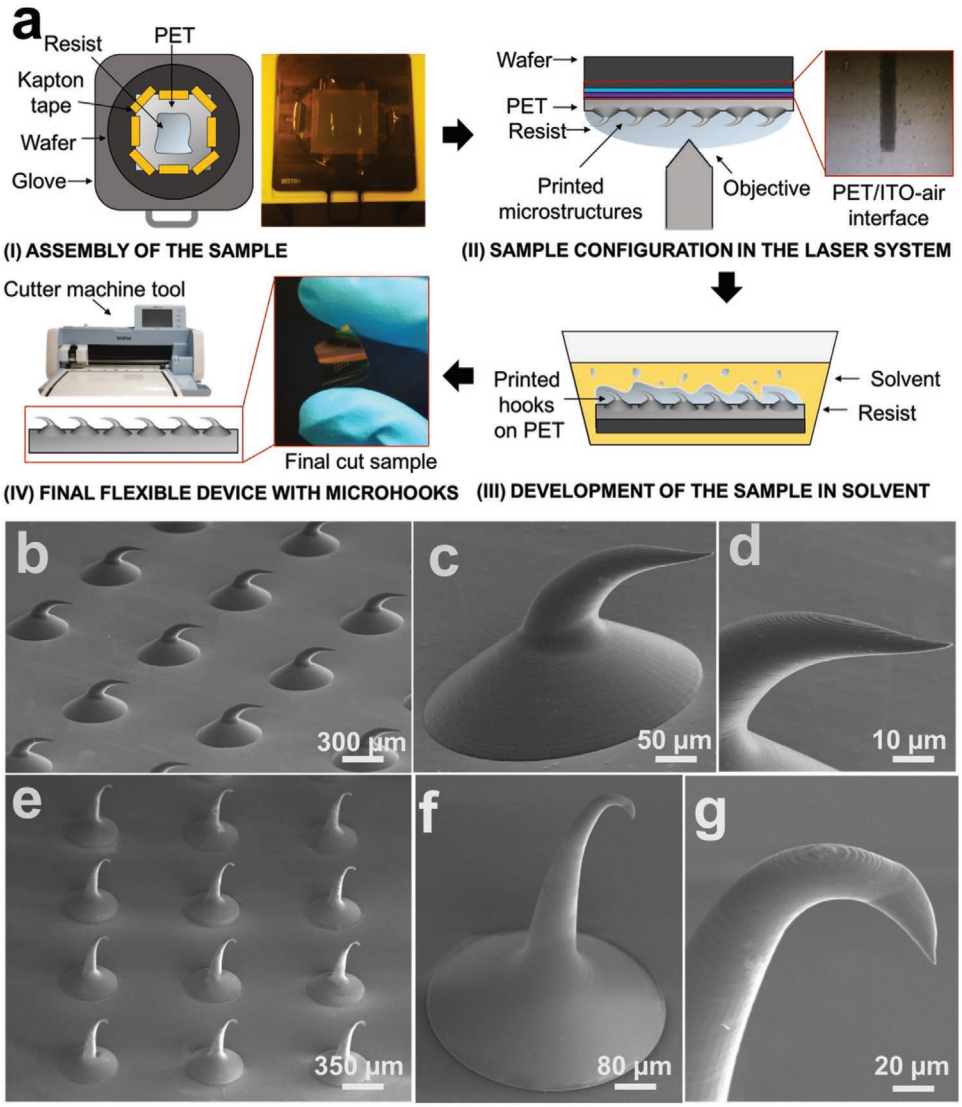

Figure 2. Fabrication of micropatterned *G. aparine*-like flexible mechanical interlockers using direct laser lithography (DLL). a) Microfabrication steps: I) assembly of the sample: schematic (right) and real (left) view assembly of flexible PET with IP-S resist on silicon wafer substrate, II) sample configuration in the laser system: 3D printing of hook array on flexible PET using Direct Laser Lithography (DLL), III) printed sample in solvent: samples were developed in SU-8 and washed with isopropanol and water, and IV) final flexible device with microhooks: the micropatterned devices are cut into squares using a professional cutter. b–g) Microfabrication results of b–d) abaxial and e–g) adaxial hooks (b,e) SEM pictures of the array and c,f) single hooks and d,g) detail of the tip).

is supported also from our mathematical model results, where abaxial hooks can hold more than 0.25 N in vertical direction (represented by the arrow in Figure S4a, Supporting Information), differently from adaxial hooks which can hold only 0.10 N (Figure S4b, Supporting Information). Furthermore, these different behaviors are more highlighted in the detachment tests on fabrics, where the downward orientation of abaxial hooks tip can lead to a greater engagement of fibers.

Figure S7 in the Supporting Information shows an example of the typical cyclic behavior of the hooks during pull-off tests.

Our results showed comparable detachment forces to other plant-inspired dry adhesives tested on the same Velcro-loop fabric substrates by applying a preload of 1 N, where the maximum detachment force is 0.03 N (refer to Table S1, Supporting Information).[7] Microscopy investigations showed that low preloads did not damage the abaxial and adaxial hook arrays after pull-off tests (e.g., at 0.02 or 0.1 N; Figure S8, Supporting Information). Applying higher preloads in our pull-off tests on textile fabrics led to some damage.

2.3.2. Frictional Properties

Two different types of experiments were carried out to investigate the shear forces of the micropatterned prototypes (Figure 3a, in captions II and III). In the first set of shear force experiments, we investigated the friction forces of the prototypes in the absence of significant preload conditions. Our aim was to characterize our devices in natural-like *G. aparine* plant conditions, which could be important in low-weight microrobotics applications.

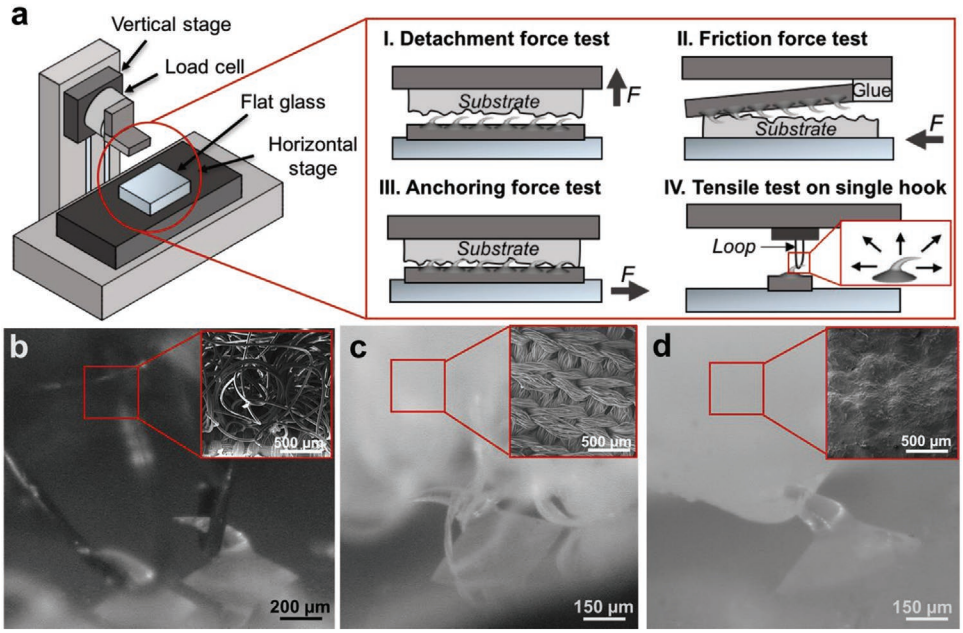

Figure 3. a) Experimental setup for all the tests, including detachment, friction, and anchoring force tests on micropatterned adhesives and single hooks. Microscope images of abaxial hooks interlocking with b) Velcro-loop fabric, c) polyester fabric, and d) artificial skin tissue. The inset shows a scanning electron microscope view of b) Velcro-loop fabric, c) polyester fabric, and d) artificial skin tissue.

During the friction force experiments, the flexible prototypes were brought into contact (without a precise preload) with several substrates with different textures and/or degrees of roughness (Figure 3a, in caption II and Figure S6, Supporting Information). The average surface roughness value (R_a) of the different substrates used for the friction force experiments, such as their profile analysis obtained using conventional contact or noncontact methods,[38] are reported in Table S4 and Figure S9 in the Supporting Information.

The experiments assessed the friction properties of the prototypes both against and toward the direction of the orientation of the hooks, similarly to the protocol used to investigate the frictional properties of the natural *G. aparine* leaves.[26] When the adhesives with abaxial or adaxial hooks were pulled toward the direction of the orientation of the hooks, significant friction forces were generated (**Figure 5**a,b for abaxial and adaxial hooks, respectively). A typical force–displacement curve is reported in Figure S10a in the Supporting Information, where each peak indicates the "transitory interlocking" of the hooks with the substrate. As with the natural hooks,[26] the mean friction forces generated by the adhesives with the abaxial hooks were much higher than the forces with the adaxial hooks (Figure 5a,b).

Figure 5a reports the friction forces generated by the prototypes with abaxial hooks, which ranged from 0.11 ± 0.04 N cm^{-2} on the low roughness abrasive material (grade P1200, R_a = 6.3 µm) to 3.3 ± 1.3 N cm^{-2} on the polyester fabric (with "well-organized" woven fibers). On the other hand, the friction

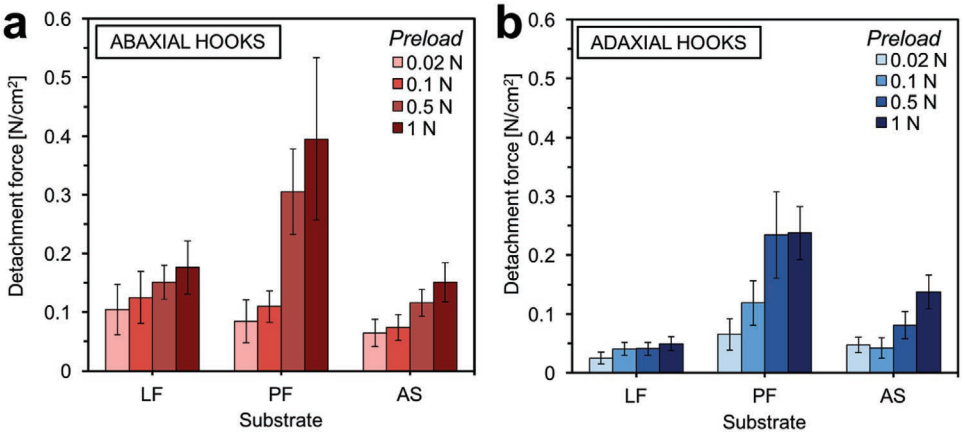

Figure 4. Maximum detachment force tests on micropatterned devices. a) Abaxial and b) adaxial hooks were pulled off different artificial surfaces, including textiles with different textures (Velcro-loop fabric (LF) and polyester fabric (PF)) and artificial skin tissues (AS) corresponding to four different preload values. The devices have a hook density of 156 hooks cm^{-2}.

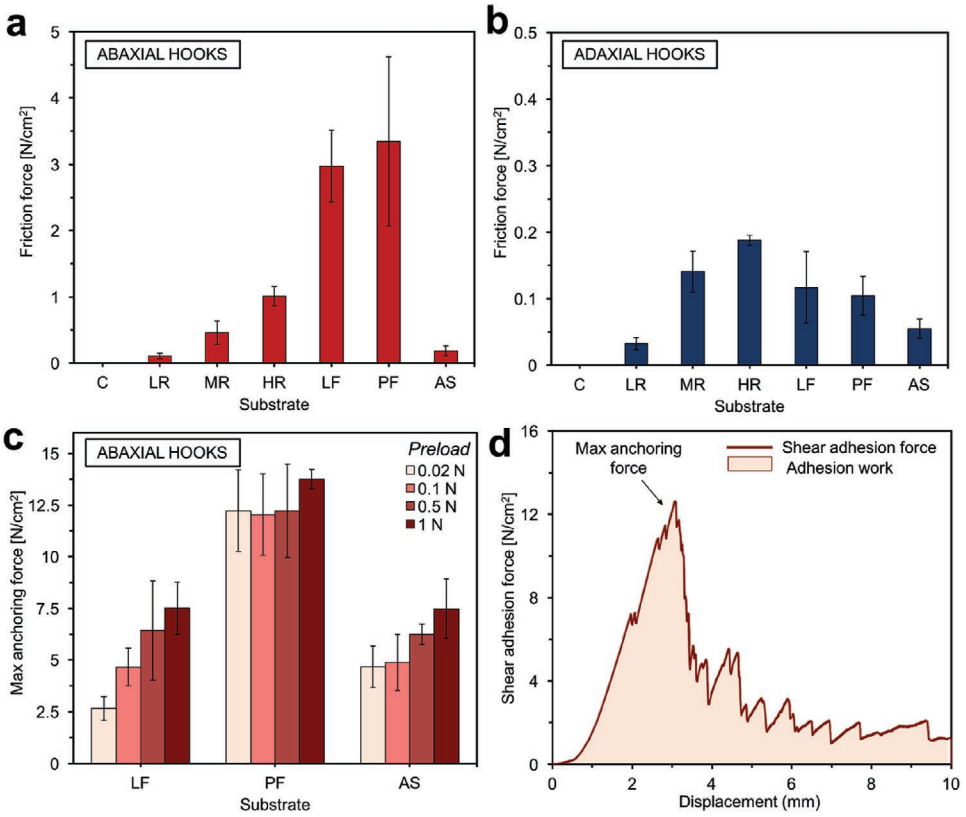

Figure 5. Shear attachment force tests on micropatterned devices. a) Friction forces generated by mechanical interlocking with a) abaxial or b) adaxial hooks pulled in the direction of the hook orientation on several artificial surfaces, including glass smooth surface as control C) (R_a = 0.00093 µm), abrasive materials at different grades (from P1200 to P80) with increasing levels of roughness (low roughness (LR) with R_a = 6.3 µm; medium roughness (MR) with R_a = 28.8 µm; high roughness (HR) with R_a = 62.4 µm), fabric textiles with different textures (Velcro-loop fabric (LF) with "messy" looped fibers and polyester fabric (PF) with "well-organized" woven fibers) and soft rough artificial skin tissues (AS) (R_a = 7.6 µm). The average roughness (R_a) of the different substrates is reported in Table S4 in the Supporting Information. c) Max shear locking forces at different preloads generated by the mechanical interlocker with abaxial hooks in the interlocking direction on different artificial surfaces, including textiles with different textures (Velcro-loop fabric (LF) and polyester fabric (PF)) and soft rough artificial skin tissues (AS). d) A typical plot of the shear attachment forces generated by the mechanical interlocker with abaxial hooks on the polyester substrate during measurement in the locking direction. The preload was 0.02 N. The maximum anchoring force was determined as the maximum force peak during the test. The devices have a hook density of 156 hooks cm^{-2}.

forces generated by the prototypes with adaxial hooks ranging from 0.03 ± 0.01 N cm^{-2} on the low roughness abrasive material (grade P1200, R_a = 6.3 µm) to 0.19 ± 0.01 N cm^{-2} on the high roughness abrasive material (grade P80, R_a = 62.4 µm) (Figure 5b). As a control, we tested the friction forces generated by the prototypes also on a glass-smooth substrate (R_a = 0.00093 µm), where, as expected, no relevant friction forces were generated due to the impossibility of mechanical interlocking with the glass (Figure 5a,b).

In general, the increase of the degree of roughness leads to higher values of friction forces in both prototypes with abaxial and adaxial hooks when pulled over the different abrasive materials or soft skin tissues. In the case of fabrics, the adaxial hooks can more easily slide-off from looped or woven fibers (thus, producing lower friction forces) due to their slender geometry, compared to abaxial hooks.

In addition, when the prototypes with abaxial or adaxial hooks were pulled against the direction of the orientation of the hooks, the general friction forces were minimal or negligible (see the example in Figure S10b, Supporting Information).

2.3.3. Anchoring Properties

In the second set of shear force experiments, we investigated the maximum anchoring force (i.e., the maximum shear locking force) obtained by the micropatterned devices when a normal preload was applied to ensure that the two surfaces overlapped. In these experiments, the devices strongly interlocked or penetrated the substrates, which included commercial textile fabrics, such as polyester and Velcro-looped part, and artificial skin tissues, without releasing them (unlike the friction force tests explained above where the hooks "temporarily interlocked" the substrate and then released it). After a normal preload, a vertical displacement at a constant speed was applied toward the direction of hook orientation in order to pull the hooks away from the contact substrates (Figure 3a, caption III and Figure 3b–d). The micropatterned adhesives with abaxial hooks exhibited strong direction-dependent shear locking forces. The maximum shear locking forces varied among the different substrates, ranging from 7.49 ± 1.42 N cm^{-2} on artificial skin tissues to 13.76 ± 0.47 N cm^{-2} on polyester fabrics. The shear attachment forces increased with the increase in

the preload on looped fabrics and artificial skin and remained constant on polyester fabrics (Figure 5c), where lower preload is enough to ensure a proper interlocking between hooks and polyester woven fibers in shear direction.

Figure 5d shows an example of the force–displacement curves of the abaxial hooks on polyester fabrics, where a maximum anchoring force was obtained after a displacement of 2 mm. The typical force–displacement curves obtained are reported in Figure S12a in the Supporting Information.

Our maximum anchoring force experiments were also performed with an artificial adaxial hook array. As expected, these tests revealed much lower shear locking forces than the abaxial ones (Figures S11 and S12b, Supporting Information). Different modes of hook failure were observed after the tests, typically at the tip or at the basal part (Figure S13, Supporting Information).

Achieving a strong soft tissue reversible attachment is fundamental for clinical applications and for preventing glue-based acrylic adhesives thus minimizing skin tissue damage.[39] To date, novel devices for reversible attachment on skin have been developed inspired by gecko or insect-like hierarchical architectures,[14,40] microneedles of endoparasitic worms,[10] octopus suction cups,[15] and the embryonic wound contraction of chicken.[41]

Although other adhesives with hook-like structures have been developed,[42] this paper reports the first example of direction-based hooks that can penetrate inside skin tissue.

Other examples of bioinspired solutions for skin interlocking (i.e., microneedle adhesives), reach a detachment force of up to ≈ 4.5 N cm^{-2}.[10] On the other hand, our different strategy using climbing plant-inspired directional hooks for penetration inside the tissue provide a novel solution for direction-based reversible attachment, with great shear attachment strength results of up to $F_{\parallel} \approx 7.5$ N cm^{-2}.

High shear attachment is also fundamental for the textile industry. Shear attachment experiments performed on typical commercial Velcro[11,37] showed an $F_{\parallel} \approx 4.9$–14 N cm^{-2}.[9] On the other hand, our prototypes with abaxial microhooks reached up to $F_{\parallel} \approx 7.5$ N cm^{-2}, when tested on Velcro-loop fabric and up to $F_{\parallel} \approx 13.8$ N cm^{-2} when tested with polyester fabric. We believe our prototypes are thus a suitable alternative for the hook part of microfasteners.

2.4. Mechanical Properties of Individual Artificial Hooks

We carried out pull-off experiments to measure the contact separation force of single artificial hooks by applying loads with different orientations[26,31] (Figure 3, caption IV and Figure S14, Supporting Information). As with natural hooks,[26] the contact separation forces exerted by our artificial abaxial hooks were much higher than the forces exerted by adaxial hooks in all the tested load orientation conditions (**Figure 6**). Our hooks also had a higher contact separation force than their natural counterparts,[26] probably due to the high stiffness of the constitutive material. The maximum contact separation force of the artificial abaxial hooks was 0.26 ± 0.03 N when hooks were pulled against the direction of the hook orientation (0°). The greater the pulling angle, the lower the contact separation force (up to 180° where there is no more interlocking since the hooks slide off of the loop), as shown in Figure 6.

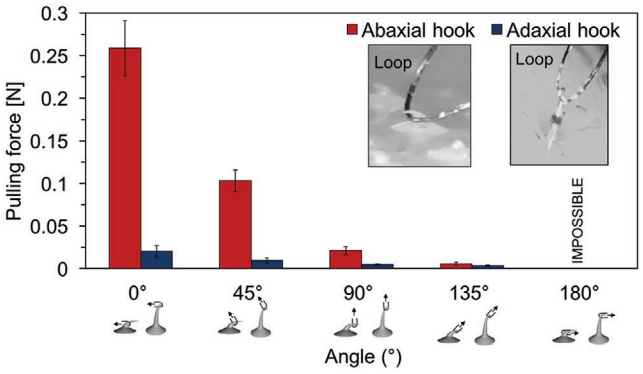

Figure 6. Pull-off forces for individual artificial abaxial (red column) and adaxial (blue column) hooks in relation to loads with different orientations. Inset: Microscope images of the abaxial and adaxial hooks pulled using a steel-wire loop.

Our artificial adaxial hooks behaved similarly and the contact separation forces decreased proportionally by tuning the angle from 90° against the direction of hook orientation to 45° toward the direction of the hook orientation (Figure 6). The performances of individual hooks under different load orientations were recorded with a portable microscope camera (see Figure S15 for abaxial hooks and Figure S16 for adaxial hooks, Supporting Information).

In general, both the artificial abaxial and adaxial hooks slide off without failure when subjected to a vertical load or to 45° against or toward the hook orientation (Figures S15c-l and S16c-l, Supporting Information). On the other hand, failure or detachment from the flexible substrate was observed when hooks were subjected to parallel forces with respect to the hook orientation (Figures S15a,b and S16a,b, Supporting Information). This was expected, since using the formula reported in Equation (S1) in the Supporting Information to compute the mechanical stress of the hook, the maximum shear stress due a load of 0.1 N applied at 45° on the abaxial hook is about 56 MPa (far below the shear strength of the material), due to the fact that the load is applied at a section with diameter ≈55 µm. The hook is thus not able to break in this condition. The same holds for a load of 0.25 N applied at 0°: since the diameter of the section is greater than 85 µm, the resulting shear stress would be less than 66 MPa. With regard to the adaxial hook, the flexibility of its apical part enables the loop to slide off along the hook, without causing fractures (see the Supporting Information).

Interestingly, the experimental forces obtained for individual artificial abaxial hooks (which ranged from 0.005 to 0.26 N according to the load direction) are comparable to the theoretical force for individual Velcro hooks (0.17 N).[9,43] This thus highlight that our bioinspired hooks are an excellent alternative for future mechanical interlockers.

2.5. Mobile Miniaturized Car with Adhesive Tape-Like Direction-Based Hooks

Several climbing robots with spine-like hooks or friction anisotropy-based microdevices have been developed for climbing over rough surfaces.[18,19,20,21,44] For instance, arrays of miniature spines can catch surface asperities of building surfaces (i.e., brick and concrete walls), reaching remarkable forces up

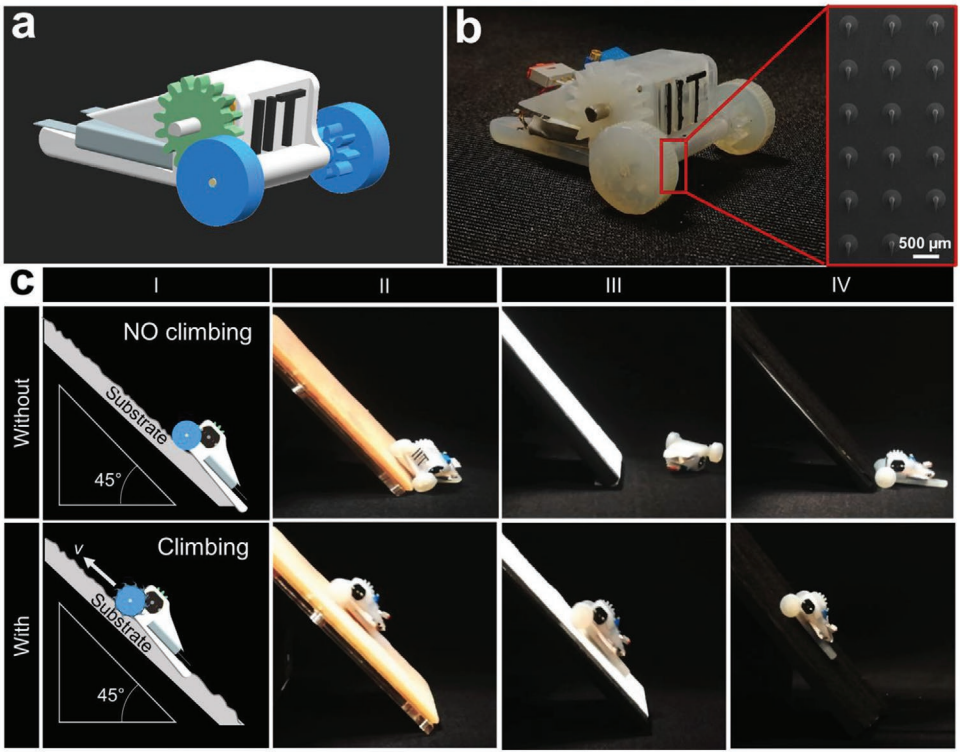

Figure 7. Mobile device with direction-based microhooks for climbing on rough surfaces. a) 3D CAD model of the mobile device. b) Mobile device with micropatterned adhesives fixed to the two wheels. Inset: A scanning electron microscope image of the direction-based microhooks printed on the flexible Mylar sheet (scale bar: 500 µm). c,I) Schematic and II–IV) pictures of the mobile device without (upper side) and with (lower side) microhooks climbing on the tested rough surfaces, II) artificial skin, III) polyester, and IV) loop fabric. The arrow indicates the climbing direction of the mobile platform.

to 1–2 N for each spine.[18,20] However, only a few examples of climbing robots have been reported for specific applications, such as textile and soft skin tissue interlocking.[45]

To demonstrate the proof of concept for terrestrial robotic applications, the climbing capabilities of a 25 g mobile car was tested on inclined rough slopes (**Figure 7**). First, the tested substrates, such as textile fabrics and skin tissue, were fixed onto a 45° inclined slope and then, the performance of the mobile mini-car was tested with and without hooks. Specifically, a flexible adhesive tape with direction-dependent micropatterned abaxial hooks was developed and fixed to the two wheels of the mobile car (Figure 7a,b). Without hooks, the car was not able to climb on the inclined slopes (upper panel in Figure 7c and Movie S4, Supporting Information); however with hooks, the car easily climbed over all the selected substrates up to a maximum 45° inclined slope, demonstrating the feasibility of the smart flexible device for climbing robot applications (lower panel in Figure 7c and Movie S4, Supporting Information). In order to climb up to horizontal surfaces, a similar ratcheting actuation used in microspine-based robots (i.e., SpinyBot)[18] could be integrated into our prototypes to better control the function between attachment and detachment at a small scale.

3. Conclusions

We have developed a novel climbing plant-inspired 3D micropatterned flexible mechanical interlocker that can perform reversible attachment to different rough substrates. Multiphoton lithography was used to fabricate 3D patterns of optimized bioinspired hooks onto a flexible substrate, ensuring high reproducibility and scalability. The patterned surfaces with artificial abaxial and adaxial hooks showed encouraging normal attachment forces ranging from a minimum of ≈0.025 N cm^{-2} to a maximum of ≈0.4 N cm^{-2} in relation to the different types of artificial hooks, the contact rough surfaces, and the preload applied during the tests.

The best results were obtained with the prototypes with abaxial hooks, which proved to have high frictional forces and strong shear locking attachment to the different substrates (up to $F_{//} \approx 7.5$ N cm^{-2} to soft skin tissues and up to $F_{\perp} \approx 13.8$ N cm^{-2} to polyester textiles).

In this paper we have also proposed a novel strategy to equip a miniaturized mobile platform with directional microhooks for climbing on textiles and soft skin tissues, thereby suggesting future avenues for a new generation of climbing robots.

Our results demonstrated that 3D multiphoton lithography in combination with other microfabrication techniques (e.g., micromolding) offers high flexibility to exploit the same procedure on different substrates and/or materials. For instance, stretchable med-patches with directional microhooks for skin tissue interlocking could be developed just by changing the substrate used. Also, new types of microsnap fastener for textiles could be microfabricated.

We believe that our novel climbing plant-inspired mechanical interlocker has great potential to benefit a wide range of fields, from basic research to applied science.

4. Experimental Section

Materials: *G. aparine* L. plants were purchased from a nursery. For the attachment tests, smooth glass for the control (76 mm × 50 mm, VWR), abrasive paper sheets (P1200, P180, P80 by 3M), looped fabric fasteners (Velcro Stick On Tape, Velcro Ltd.), polyester fabric (100% textured polyester, Polynit Heatseal Wipes, Contec, Inc.), and artificial skin tissues (Basic Tissue Plate, SynDaver) were used as substrates. The average roughness (R_a) of the different substrates was quantified using a 3D noncontact optical profilometry system (Leica DCM 3D, Leica Microsystems) in case of rough abrasive materials and skin tissues. Instead, a contact stylus profilometer (KLA-Tencor P-6) was used in case of smooth glass. R_a is considered as the arithmetic mean deviation of the profile.

Semi-dry artificial skin tissues were conserved in distilled water and soap at room temperature. Before all mechanical tests, the water was removed from the skin surface using blotting paper and an air gun.

Time-Lapse Observations: *G. aparine* L. plants were moved to the growth chamber (temperature 25 °C, 60% humidity, 16 h-8 h light-dark cycle). In the growth chamber, *G.aparine* L. was placed close to a host plant (*Salvia officinalis* L.) and its climbing behavior was recorded for 5 d using time-lapse photography at 10 min intervals with a digital camera (Pentax WG-3). The acquired images were postprocessed using VirtualDub software.

Digital Microscope: Pictures and videos of the natural and artificial abaxial and adaxial leaf hooks were obtained with a Hirox KH-7700 digital microscope.

Scanning Electron Microscopy (SEM): Before imaging, the freshly cut leaves of *G. aparine* L. were chemically fixed in 2.5 % glutaraldehyde and then dehydrated through a graded series of ethanol dilutions. To preserve the 3D structures, the plant and artificial skin specimens were treated in a critical point dryer instrument (Autosamdri-931, Tousimis) in stasis mode. For all the other artificial samples no preparation was required.

All samples were mounted onto aluminum stubs and coated with a 15 nm gold layer using a sputter coater (Quorum Q150R ES, United Kingdom). Surface topography images were obtained with an EVO LS10 scanning electron microscope (Zeiss, Germany) at an accelerating voltage of 5–10 kV.

Bioinspired Design and Modeling of Microhooks: For the bioinspired design, the main geometrical parameters, such as length and diameter, were extracted from the SEM images of natural leaf hooks. Based on the morphometric datasets, the selected material for the fabrication, the maximum force that hooks achieve in nature, and the structural response to an assigned load were computed. This computation entailed implementing the set of ordinary differential equations (ODEs) reported in ref. [28] solved over a curvilinear coordinate running along the longitudinal axis of the hook. While some geometrical parameters were assigned, such as the length of the projection of the hook along the direction of the substrate, others were treated as design variables; in particular, the shape of the axis of the abaxial hooks was not defined a priori.

The values of the design variables were computed by solving a constrained optimization problem. The objective was to find the optimal geometry of the hooks such that they would be able to withstand a load with an assigned amplitude and direction.

The model was implemented in Matlab, using the Global Optimization Toolbox (see the Supporting Information). The solver used for the set of ODEs was *ode45*. All the scripts are available from the authors on request. Based on the optimization results, 3D computer aided design (CAD) models were developed in SolidWorks 2017 (Figure 1c,f).

Microfabrication Using DLL: 3D patterns of the artificial microhooks were fabricated in IP-S, Nanoscribe GmbH photoresist (Young's modulus: 4.68 GPa) on flexible Mylar plastic sheets (0.023 mm, polyethylene terephthalate, PET, RS Components, Inc.) by means of the Nanoscribe Photonic Professional (GT) system (Nanoscribe GmbH). The full microfabrication process is reported in Figure 3a.

Before printing, a nanomillimeter-thick layer of indium tin oxide (ITO) was deposited with a DC Magnetron sputtering system onto the Mylar surface to facilitate the interface detection thanks to the different refractive indexes. The other side of the Mylar sheet was then plasma-treated for 60 s (Colibrì, Gambetti Kenologia SRL) to facilitate the adhesion of the IP-S resist onto the surface of the Mylar. The treated Mylar sheet was carefully fixed with Kapton adhesive tape on a silicon wafer substrate (4′) and then, the IP-S photoresist was poured onto the Mylar. The IP-S resist was exposed to a laser beam (wavelength: 780 nm, Toptica laser source) by means of a 25X immersion objective, using a scan speed of 20 mm s^{-1} and a laser power of 28 mW. The ITO-coated Mylar/air interface was detected by the laser system. The 3D microstructures were printed in arrays of 6 by 6 microhooks at a distance of 800 µm (36 hooks, area of the array: 23.04 mm^2). The samples were developed for 20 min in a common epoxy based-negative photoresist (SU-8) developer (1-methoxy-2-propanol acetate) (MicroChem Corp), rinsed with isopropyl alcohol, washed with deionized water, and dried with air. After the development, the dried Mylar sheet with the microprinted hook structures was cut into square samples with an electronic cutting machine (ScanNCut SDX 1200, Brother USA). The overall process is summarized in Figure 2a.

Measurement of Detachment Force, Anchoring Force, Sliding Friction Force, and Contact Separation Force of Artificial Hooks: All attachment measurements were carried out using a dedicated setup with a multiaxis measurement platform, equipped with: two motorized microtranslation stages (an M-111.1DG for the vertical motion and an M-126.CG1 for the horizontal one, both controlled by C-863 Mercury Servo Controller, both produced by Physik Instrumente GmbH) and a six-axis force/torque sensor (Nano17, ATI Industrial Automation) with a resolution of 0.003 N (Figure 3a, left panel).

Four different types of tests, including pull-off attachment, shear attachment, sliding friction force, and contact separation force tests, were carried out on artificial hooks (Figure 3a). The cycles of the tests and the data acquisition (at 20 Hz with an average level of 200 samples) were managed by dedicated software developed in VB.NET (Microsoft Corp.).

For the pull-off and shear attachment tests on the hook array, the sample was placed on the bottom plate of the setup and a piece of the selected substrate (0.25 cm^2) (which included looped fabric, polyester fabric, and artificial skin tissue) was fixed to the top plate. The top plate was lowered at a speed of 0.2 mm s^{-1} until it reached a fixed preload, varying from 0.02 to 1 N.

In the pull-off attachment tests, a horizontal displacement against the direction of the hooks of 300 µm was used to promote the mechanical interlocking with the substrate. The top plate was then retracted perpendicularly at a speed of 0.5 mm s^{-1} until the final detachment.

For each test run, the mean value of the maximum force reached before the final detachment was determined over five cycles. In the shear attachment tests, a horizontal displacement against the direction of the hooks of 1 cm was applied in order to evaluate the maximum anchoring force achieved by artificial hooks on different substrates. For each test run, the maximum shear attachment force was determined to be the maximum force peaks of the force–displacement curves.

For the sliding friction force experiments on the hook array, friction forces were measured by pulling artificial flexible samples onto different substrates,[26] including sandpaper with different degrees of particle size and roughness (P1200, P180, P80), a looped fabric fastener, polyester fabric, and artificial skin tissue. The samples on the top plate were attached to a load force-cell sensor by fixing them using a custom holder. The substrates were attached onto the base plate, consisting of a motorized horizontal translation stage, which was moved horizontally both in and against the orientation of the hooks at a speed of 0.2 mm s^{-1} for 2.5 cm. The distance between the holder on the top plate (where the flexible device was attached) and the tested substrate was 1.5 mm for the sandpaper, 3 mm for the polyester fabric and artificial skin tissue, and 3.5 mm for the looped fabric fastener. For each test run, the mean value of seven force peaks of force–displacement curves was calculated (Figure S10, Supporting Information).[26]

For the contact separation force tests on a single hook, the pulling forces were measured by pulling off a wire thread loop from a single

hook using the micrometric motorized two-axis translational stages. A stainless steel insulated wire thread (25 µm diameter) loop (3–5 mm length) (Goodfellow Cambridge Ltd) was fixed to the top plate. The sample was fixed to a glass side with double-sided adhesive tape. The glass side was fixed to several inclined planes with different slopes (see Figure S14, Supporting Information). The loop, which interlocked with the hook, was pulled off at different angles (from 0° to 180°, see Figure S15 and Figure S16, Supporting Information) with respect to the sample plane (similarly to refs. [26], [32], and [34]) at a speed of 0.2 mm s^{-1}. A portable digital microscope (Dino Lite Edge digital microscope) connected to a computer was used to observe and record the mechanical behavior of the artificial hooks during the tests (see Figure S14, Supporting Information).

Design and Fabrication of the Car: The car has two active wheels for forward locomotion and a body that provides the third contact point for robot stabilization and to enable the two active wheels to rotate with respect to the ground. The device was designed in NX 11 (Siemens Product Lifecycle Management (PLM) Software) exploiting a small DC motor (CHF-GM12-N10 from Chiai Motor). The aim was to produce a frame of minimum weight. A slot was created in the frame for a lithium battery (240 mAh, 20C, Z240S20C from Zippy) connected to a switch and to a variable resistance (max 100 Ω) to tune the speed of the car. The wheels were designed with an embedded gear coupled by a second gear with the motor. The wheels were connected together by a shaft. The car, gear, and geared wheels were fabricated by 3D printing with Durable Resin (FormLabs). The total weight of the car was 25 g (motor 7 g, battery 5.9 g, other parts 12.1 g).

Demonstration of Climbing Capabilities of the Car: A type of adhesive tape with artificial abaxial microhooks was attached to the wheels of the car (Figure 7). Various substrates, including a looped fabric fastener, polyester fabric and artificial skin tissues were fixed to a 45° inclined glass plate. The car's climbing performance on the inclined substrates was tested with and without hooks on the wheels, while a fixed phone camera (Leica, 12 MP RGB) was used for video recording.

Supporting Information

Supporting Information is available from the Wiley Online Library or from the author.

Acknowledgements

O.T. and G.A.N. contributed equally to this work. This work was funded by the European Union's Horizon 2020 Research and Innovation Programme under Grant Agreement No. 824074 (GrowBot Project) and by the National Geographic Society (NGS) under Grant Agreement No. EC-62190T-19.

Conflict of Interest

The authors declare no conflict of interest.

Keywords

bioinspired devices, climbing robots, microhooks, reversible attachments, two photon lithography

Received: April 16, 2020
Revised: June 5, 2020
Published online:

[1] a) S. Kim, C. Laschi, B. Trimmer, *Trends Biotechnol.* **2013**, *31*, 287; b) C. Laschi, B. Mazzolai, M. Cianchetti, *Sci. Rob.* **2016**, *1*, eaah3690.
[2] a) J. F. Vincent, *Proc. Inst. Mech. Eng., Part H* **2009**, *223*, 919; b) Y. Bar-Cohen, *Bioinspiration Biomimetics* **2006**, *1*, P1; c) Z. Xia, *Biomimetic Principles and Design of Advanced Engineering Materials*, John Wiley & Sons, USA **2016**; d) I. Fiorello, E. Del Dottore, F. Tramacere, B. Mazzolai, *Bioinspiration Biomimetics* **2020**, *15*, 031001.
[3] Y. Wang, X. Yang, Y. Chen, D. K. Wainwright, C. P. Kenaley, Z. Gong, Z. Liu, H. Liu, J. Guan, T. Wang, *Sci. Rob.* **2017**, *2*, eaan8072.
[4] a) F. Tramacere, M. Follador, N. Pugno, B. Mazzolai, *Bioinspiration Biomimetics* **2015**, *10*, 035004; b) S. Sareh, K. Althoefer, M. Li, Y. Noh, F. Tramacere, P. Sareh, B. Mazzolai, M. Kovac, *J. R. Soc., Interface* **2017**, *14*, 20170395.
[5] a) H. Jiang, E. W. Hawkes, C. Fuller, M. A. Estrada, S. A. Suresh, N. Abcouwer, A. K. Han, S. Wang, C. J. Ploch, A. Parness, *Sci. Rob.* **2017**, *2*, eaan4545; b) P. Glick, S. A. Suresh, D. Ruffatto, M. Cutkosky, M. T. Tolley, A. Parness, *IEEE Rob. Autom. Lett.* **2018**, *3*, 903.
[6] J. Jiao, F. Zhang, T. Jiao, Z. Gu, S. Wang, *Adv. Sci.* **2018**, *5*, 1700787.
[7] H. G. Andrews, J. P. S. Badyal, *J. Adhes. Sci. Technol.* **2014**, *28*, 1243.
[8] I. Fiorello, O. Tricinci, A. K. Mishra, F. Tramacere, C. Filippeschi, B. Mazzolai, presented at *Conf. Biomimetic Biohybrid Syst.*, Paris, France, July **2018**.
[9] L. M. Mariani, C. M. Esposito, P. J. Angiolillo, *Tribol. Lett.* **2014**, *56*, 189.
[10] S. N. Gorb, *Philos. Trans. R. Soc., A* **2008**, *366*, 1557.
[11] M. G. De, *Google Patent No. 3,009,235*, **1961**.
[12] a) C. Pang, T. i. Kim, W. G. Bae, D. Kang, S. M. Kim, K. Y. Suh, *Adv. Mater.* **2012**, *24*, 475; b) H. E. Jeong, J.-K. Lee, H. N. Kim, S. H. Moon, K. Y. Suh, *Proc. Natl. Acad. Sci. USA* **2009**, *106*, 5639.
[13] C. Pang, D. Kang, T.-i. Kim, K.-Y. Suh, *Langmuir* **2012**, *28*, 2181.
[14] D. M. Drotlef, M. Amjadi, M. Yunusa, M. Sitti, *Adv. Mater.* **2017**, *29*, 1701353.
[15] S. Baik, J. Kim, H. J. Lee, T. H. Lee, C. Pang, *Adv. Sci.* **2018**, *5*, 1800100.
[16] S. N. Gorb, *Philos. Trans. R. Soc., A* **2008**, *366*, 1557.
[17] a) H. Afrisal, S. H. Sadati, T. Nanayakkara, presented at 2016 IEEE Int. Conf. Inf. Autom. Sustainability (ICIAfS), **2016**; b) S. N. Gorb, V. L. Popov, *Physical and Engineering Sciences* **2002**, *360*, 211; c) J. Williams, S. Davies, S. Frazer, *Tribol. Lett.* **2007**, *26*, 213.
[18] A. T. Asbeck, S. Kim, A. McClung, A. Parness, M. R. Cutkosky, presented at IEEE ICRA **2006**.
[19] a) W. R. Provancher, J. E. Clark, B. Geisler, M. R. Cutkosky, *Climbing and Walking Robots*, Springer, Berlin, Germany **2005**, p. 961; b) A. Parness, C. McKenzie, *Ind. Rob.* **2013**, *40*; c) Y. Liu, S. Sun, X. Wu, T. Mei, *J. Bionic Eng.* **2015**, *12*, 17.
[20] S. Kim, A. T. Asbeck, M. R. Cutkosky, W. R. Provancher, presented at *12th Int. Conf. Adv. Rob.*, Seattle, WA, July **2005**.
[21] H. Jiang, S. Wang, M. R. Cutkosky, *Int. J. Rob. Res.* **2018**, *37*, 669.
[22] a) S. Wang, H. Jiang, M. R. Cutkosky, presented at *Intell. Rob. Syst. (IROS)*, Seoul, Korea, October **2016**; b) A. Parness, presented at *2011 IEEE Int. Conf. Rob. Autom.*, Shangai, China, May **2011**; c) I. Fiorello, F. Meder, O. Tricinci, C. Filippeschi, B. Mazzolai, presented at *Conf. Biomimetic and Biohybrid Syst.*, Nara, Japan, July **2019**.
[23] a) C. Darwin, *Bot. J. Linn. Soc.* **1865**, *9*, 1; b) S. Isnard, W. K. Silk, *Am. J. Bot.* **2009**, *96*, 1205; c) N. Rowe, T. Speck, *New Phytol.* **2005**, *166*, 61; d) N. Rowe, S. Isnard, T. Speck, *J. Plant Growth Regul.* **2004**, *23*, 108.
[24] N. P. Rowe, T. Speck, *Ecol. Lianas* **2014**, *7*, 323.
[25] A. J. Bowling, H. B. Maxwell, K. C. Vaughn, *Protoplasma* **2008**, *233*, 223.
[26] G. Bauer, M. C. Klein, S. N. Gorb, T. Speck, D. Voigt, F. Gallenmüller, *Proc. Biol. Sci.* **2011**, *278*, 2233.

[27] K. J. Niklas, *Curr. Biol.* **2011**, *21*, R199.
[28] E. Tufekci, A. Arpaci, *Struct. Eng. Mech.* **2006**, *22*, 131.
[29] N. Anscombe, *Nat. Photonics* **2010**, *4*, 22.
[30] a) A. Marino, C. Filippeschi, V. Mattoli, B. Mazzolai, G. Ciofani, *Nanoscale* **2015**, *7*, 2841; b) O. Tricinci, T. Terencio, B. Mazzolai, N. M. Pugno, F. Greco, V. Mattoli, *ACS Appl. Mater. Interfaces* **2015**, *7*, 25560.
[31] Q. Chen, S. N. Gorb, E. Gorb, N. Pugno, *J. R. Soc., Interface* **2013**, *10*, 20120913.
[32] E. Gorb, S. Gorb, *Plant Physiol. Biochem.* **2002**, *40*, 373.
[33] F. Gallenmüller, A. Feus, K. Fiedler, T. Speck, *PLoS One* **2015**, *10*, e0143850.
[34] E. Gorb, V. Popov, S. Gorb, *WIT Trans. Ecol. Environ.* **2002**, *3*, 151.
[35] I. Bernardeschi, O. Tricinci, V. Mattoli, C. Filippeschi, B. Mazzolai, L. Beccai, *ACS Appl. Mater. Interfaces* **2016**, *8*, 25019.
[36] A. M. Goodman, *Ann. Bot.* **2004**, *95*, 475.
[37] M. G. De, *Google U.S. Patent 2,717,437*, **1955**.
[38] a) P. Leroux, Sandpaper Roughness Measurement using 3D Profilometry (Technical Report) **2014**; b) S. A. Mooneghi, S. Saharkhiz, S. M. H. Varkiani, *J. Eng. Fibers Fabr.* **2014**, *9*, 1.
[39] J. M. Karp, R. Langer, *Nature* **2011**, *477*, 42.
[40] S. Baik, H. J. Lee, D. W. Kim, J. W. Kim, Y. Lee, C. Pang, *Adv. Mater.* **2019**, *31*, 1803309.
[41] S. Blacklow, J. Li, B. Freedman, M. Zeidi, C. Chen, D. Mooney, *Sci. Adv.* **2019**, *5*, eaaw3963.
[42] C. Hollinsky, T. Kolbe, I. Walter, A. Joachim, S. Sandberg, T. Koch, T. Rülicke, *J. Am. Coll. Surg.* **2009**, *208*, 1107.
[43] N. M. Pugno, *Appl. Phys. Lett.* **2007**, *90*, 121918.
[44] P. Manoonpong, D. Petersen, A. Kovalev, F. Wörgötter, S. N. Gorb, M. Spinner, L. Heepe, *Sci. Rep.* **2016**, *6*, 39455.
[45] a) H. Lu, M. Zhang, Y. Yang, Q. Huang, T. Fukuda, Z. Wang, Y. Shen, *Nat. Commun.* **2018**, *9*, 1; b) K. A. Daltorio, T. E. Wei, A. D. Horchler, L. Southard, G. D. Wile, R. D. Quinn, S. N. Gorb, R. E. Ritzmann, *Int. J. Rob. Res.* **2009**, *28*, 285.